The structure of short- and medium-range order of Fe-rich amorphous Fe-La alloys

1989 J. Phys.: Condens. Matter 1 2077

(http://iopscience.iop.org/0953-8984/1/11/016)

J. Phys.: Condens. Matter 1 (1989) 2077–2086. Printed in the UK

The structure of short- and medium-range order of Fe-rich amorphous Fe–La alloys

M Matsuura†, H Wakabayashi‡, T Goto§, H Komatsu‖ and K Fukamichi‖

† Miyagi National College of Technology, Nodayama, Natori-shi, Miyagi 981-12, Japan

‡ Tokyo Institute of Technology, Department of Applied Physics, Meguro Tokyo 152, Japan

§ The Institute for Solid State Physics, The University of Tokyo, Tokyo 106, Japan

‖ Department of Material Science, Faculty of Engineering, Tohoku University, Sendai 980, Japan

Received 12 August 1988

Abstract. The ferromagnetic state of iron-rich amorphous Fe_xLa_{1-x} alloys (a-Fe_xLa_{1-x}) is known to become unstable with increasing iron concentration and at $x = 0.9$ a cusp characteristic of a spin glass appears in the AC susceptibility. In order to elucidate the correlations between the magnetic properties and the structure, we measured both large-angle and small-angle x-ray scatterings for a-Fe_xLa_{1-x} ($0.65 \leqslant x \leqslant 0.9$) alloys. From large-angle scattering measurements, interatomic distances and partial coordination numbers between Fe–Fe, Fe–La and La–La atoms were determined. The Fe–Fe interatomic distances for these alloys are all very close to the critical value (=2.54 Å) at which an antiferromagnetic exchange competes with a ferromagnetic one. The Fe–Fe coordination number of 8.6 for a-$Fe_{0.9}La_{0.1}$ was found to be close to 8.8 for crystalline $(Fe_{0.86}Al_{0.14})_{13}La$ alloy where the ferromagnetic ordering collapses and the antiferromagnetic one dominates. The small-angle scattering for a-$Fe_{0.9}La_{0.1}$ shows pronounced high intensity in contrast to those for others ($x = 0.7$ and 0.8). This fact suggests that inhomogeneous regions exist in a-$Fe_{0.9}La_{0.1}$. From the correlation function $\gamma(r)$ and Q-invariant $2\pi^2\gamma(0)$, we conjecture that the inhomogeneous regions consist of iron clusters whose size is widely distributed and their volume fraction is estimated to be about 2%. The correlations of iron clusters with the spin glass state of a-$Fe_{0.9}La_{0.1}$ are discussed.

1. Introduction

For most Fe-based amorphous alloys the ferromagnetic state tends to be unstable and spin-glass-like behaviour appears when the concentration approaches pure iron (Fukamichi *et al* 1988, 1989). For example, the AC susceptibiltiy of a-Fe_xLa_{1-x} alloys ($0.7 \leqslant x \leqslant 0.875$) at low field ($H = 1.0$ Oe) shows that the Curie temperature, T_C, decreases from 287 K to 230 K with increasing Fe concentration (Wakabayashi 1988). An alloy in this concentration region exhibits a transition from a ferromagnetic to a spin glass state at a freezing temperature T_f ($<T_C$) below which the AC susceptibility decreases. Furthermore, the AC susceptibility of a-Fe_xLa_{1-x} alloys with $x \geqslant 0.9$ shows a cusp typical of a spin glass. In addition to a-FeR alloys, other Fe-rich amorphous alloys

0953-8984/89/112077 + 10 $02.50

Table 1. X-ray weighting factors $W_{ij}/\langle f^2\rangle$ for distribution functions of Fe_xLa_{1-x} alloys.

	$Fe_{0.9}La_{0.1}$	$Fe_{0.85}La_{0.15}$	$Fe_{0.75}La_{0.25}$	$Fe_{0.65}La_{0.35}$
W_{Fe-Fe}	0.65	0.52	0.33	0.21
$2W_{Fe-La}$	0.31	0.40	0.48	0.50
W_{La-La}	0.04	0.08	0.18	0.29

such as Fe–B (Fukamichi 1983) and Fe–Zr (Saito *et al* 1986) are known to have a ferromagnetic state that becomes unstable as the Fe concentration approaches that of pure iron.

The reason why the ferromagnetic state of Fe-based amorphous alloys becomes unstable as the Fe concentration approaches that of pure iron has been discussed in connection with FCC γ-Fe; since a short-range structure of an amorphous pure metal which can be well represented by the dense random packing of hard spheres is similar to a FCC one, amorphous pure iron should have antiferromagnetic couplings as in FCC γ-Fe. However, the values of the Fe–Fe interatomic distance of an amorphous alloy are not unique but distributed, so the coexistence of ferro- and antiferro-couplings is likely to occur. Furthermore, the concentration region where ferromagnetic instability takes place is close to the critical concentration of amorphisation for Fe-based alloys (Fukamichi and Hiroyoshi 1985). Therefore, structural or compositional inhomogeneity is likely to occur, and this also affects the occurrence of ferromagnetic instability of Fe-rich amorphous alloys. Little work has been done, however, on the correlations between structural or compositional imhomogeneity and the ferromagnetic instability of Fe-rich amorphous alloys.

In order to elucidate how the structural changes are associated with the occurrence of the spin-glass-like behaviour for a-$Fe_{0.9}La_{0.1}$ and with the ferromagnetic instability of a-Fe_xLa_{1-x} ($0.65 \leq x < 0.9$) alloys, we have measured large-angle (LAXS) and small-angle (SAXS) x-ray scatterings. Because LAXS provides structural information on the short-range order whereas SAXS does so on the medium-range order, it is advantageous to use both methods for structural studies of amorphous alloys. Furthermore, as discussed in our previous work (Matsuura *et al* 1988a, 1988b) amorphous Fe–La alloys are fairly convenient substances for the study of the structure by x-ray diffraction because the atomic radius of La (1.88 Å) is the largest among rare-earth metals; the ratio of the Goldschmidt radius of La to that of Fe is 1.44. Moreover, the x-ray atomic form factor of the La atom is so large that the weighting factors for La–La and La–Fe correlations are considerable even in an Fe-rich concentration region (see table 1). Therefore, their partial distribution functions can be easily distinguished and deduced from a total radial distribution function without any troublesome experiments.

2. Experimental procedures and data analysis

All of the samples used for x-ray diffraction were prepared by high-rate DC sputtering, the conditions for which were as follows; the target voltage and current were 1.0 kV and 60 mA respectively, and the Ar gas pressure was 5.3 Pa. The samples were deposited on to a water-cooled Cu substrate for LAXS measurements and on to Al foil (0.015 mm thick) for SAXS ones. The sample thickness was about 0.4 mm for LAXS and 0.02–0.03 mm for SAXS. Mo Kα was used as the x-ray source. A curved quartz crystal and a zirconium

filter were used for the monochromator in the measurements of LAXS and SAXS, respectively. Since the details of the measurements and the data analysis for LAXS have been described previously (Matsuura 1986b), only a brief description of the SAXS measurements will be given below.

A Kratky camera, Rigaku 2203E, was used for the SAXS measurements. The widths of the incident and receiving slits were 0.04 and 0.08 mm, respectively. The height of the longitudinal slit was 10 mm. In order to estimate the intensity resulting from primary beam and parasitic scattering, the background intensity, $P_b(Q)$, was measured by setting a sample at the middle of a U-slit from which sample scattering does not reach the counter. The corrected intensity $P_c(Q)$ was obtained by subtracting $P_b(Q)$ from $P_s(Q)$:

$$P_c(Q) = P_s(Q) - P_b(Q). \tag{1}$$

The slit length correction assuming an infinite slit length was carried out by the method given by Guinier and Fournet (1955) and Schmidt (1976), i.e.

$$I(Q) = -\frac{2}{\lambda W_1(0)} \int_0^\infty \frac{P' \sqrt{Q^2 + u^2}}{\sqrt{Q^2 + u^2}} \, \mathrm{d}u \tag{2}$$

where Q is the wavenumber (Å^{-1}) given as $Q = (4\pi/\lambda) \sin\theta$ (θ is the scattering angle), λ the wavelength, $W_1(0)$ the slit length weighting factor and $P'(x) \equiv \mathrm{d}P(x)/\mathrm{d}x$. The absolute scattering intensity, $J(Q)$, can be determined from the scattering intensity $I(Q)$, i.e.

$$J(Q) = K_0 I(Q) \tag{3}$$

and

$$K_0 = K/\gamma_T^2 N_v (t\, \mathrm{e}^{-\mu t}) \tag{4}$$

where γ_T is the Thomson radius, N_v the number of scattering units per unit volume in sample thickness t, μ the mass absorption coefficient and K the characteristic constant of the Kratky camera given by

$$K = \kappa_{\text{poly}}(Q')(\mathrm{e}^{-\mu t})_{\text{poly}} W_1(0)/P_{\text{poly}}(Q') \tag{5}$$

where κ_{poly} is the characteristic value of the Lupolen used in the present work (=0.0168 for Mo Kα and $P_{\text{poly}}(Q')$ the observed intensity of the Lupolen at Q'(=0.042 Å^{-1}) at the same conditions as the sample measurement.

The correlation function $\gamma(r)$ and the Q-invariant $2\pi^2\gamma(0)$ defined by equations (6) and (7), respectively, are derived from the absolute scattering intensity $J(Q)$.

$$\gamma(r) = \frac{1}{2\pi^2 r} \int_0^\infty QJ(Q) \sin(Qr) \, \mathrm{d}Q \tag{6}$$

$$\gamma(0) = \frac{1}{2\pi^2} \int_0^\infty Q^2 J(Q) \, \mathrm{d}Q. \tag{7}$$

The Q-invariant (=$2\pi^2\gamma(0)$) is related to the electron density fluctuation $\Delta\rho(=\rho - \rho_0)$ and volume fraction V_f of particles by

$$\gamma(0) = \Delta\rho^2 V_f(1 - V_f) \tag{8}$$

where ρ and ρ_0 are the electron densities of particles and matrix, respectively.

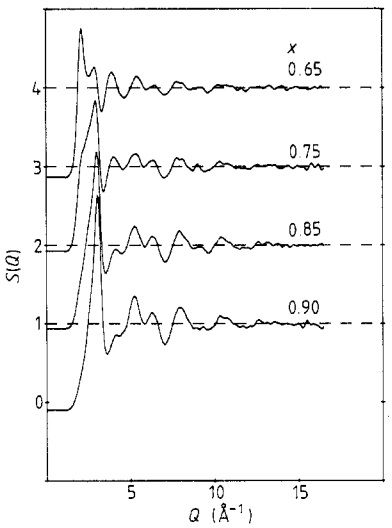

Figure 1. Faber–Ziman-type interference functions $S(Q)$ of amorphous Fe_xLa_{1-x} ($x = 0.65$, 0.75, 0.85 and 0.90) alloys.

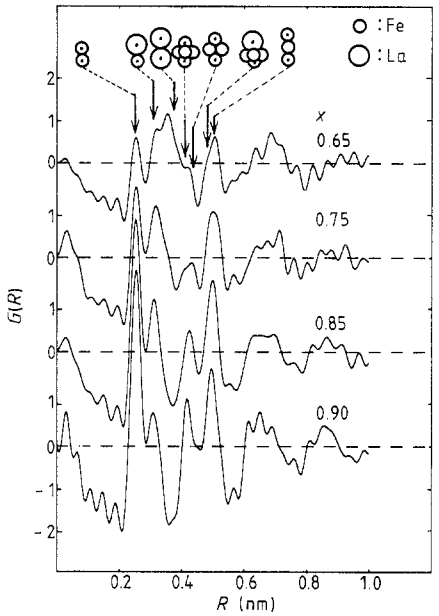

Figure 2. Reduced radial distribution functions $G(r)$ for amorphous Fe_xLa_{1-x} ($x = 0.65$, 0.75, 0.85 and 0.90) alloys. Arrows indicate the estimated interatomic distances corresponding to the illustrated atomic arrangements.

3. Results

3.1. Large-angle x-ray scattering

Figure 1 shows the Faber–Ziman-type interference functions $S(Q)$ for a-Fe_xLa_{1-x} ($x = 0.65$, 0.75, 0.85 and 0.9) alloys. Because of the large x-ray atomic form factor of the La atom, the weighting factor of the partial interference function between La atoms, W_{La-La}, increases rapidly with La concentration as shown in table 1. The intensity of the La–La interference, therefore, exceeds the Fe–Fe one with increasing La concentration and the first peak splits into a double peak at 35 at.% La.

The reduced radial distribution function $G(r)$ is defined as

$$G(r) = 4\pi r(g(r) - g_0) \tag{9}$$

where $g(r)$ is the atomic distribution function and g_0 the mean number density. It is derived from the Fourier transform of $S(Q)$, i.e.

$$G(r) = \frac{2}{\pi}\int_0^\infty Q[S(Q) - 1]\sin(Qr)\,\mathrm{d}Q. \tag{10}$$

The g_0-values are obtained from previous work (Matsuura *et al* 1988b). Resultant $G(r)$ curves are shown in figure 2. Since the ratio of the atomic radii of Fe and La, r_{La}/r_{Fe}, is relatively large, the first three peaks, i.e. Fe–Fe, Fe–La and La–La correlations, are clearly distinctive and even the second neighbours can be identified as shown in figure 2. The arrows in the figure show the estimated interatomic distances of the respective

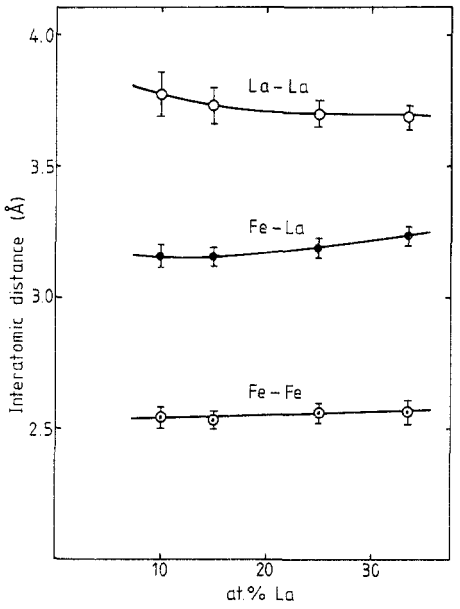

Figure 3. Concentration dependences of the interatomic distances of the first Fe–Fe, Fe–La and La–La neighbours of amorphous Fe_xLa_{1-x} alloys.

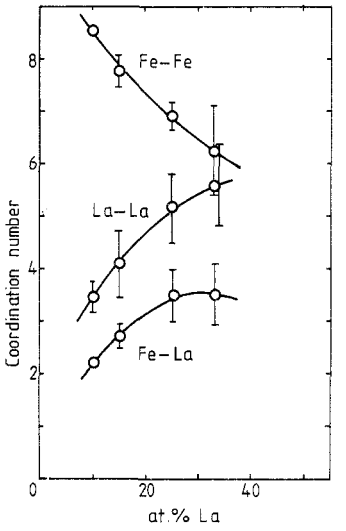

Figure 4. Partial coordination numbers of the first Fe–Fe, Fe–La and La–La neighbours against La concentration of amorphous Fe_xLa_{1-x} alloys.

atomic arrangements illustrated in the same figure. The Goldschmidt atomic radii were used in these estimations. The interatomic distances and partial coordination numbers were determined by fitting the experimental $G(r)$ curves to those of the sum of Gaussian functions. The results of the concentration dependences of the interatomic distances and the partial coordination numbers between Fe–Fe, Fe–La and La–La are shown in figures 3 and 4 respectively, and they are also listed in table 2.

The normalised order parameter η^0 defined by Cargill and Spaepen (1981) is useful in comparing the degree of chemical ordering in a system with different compositions. The estimated order parameters are listed in table 2 and are plotted in figure 5. These results indicate that the chemical ordering of a-Fe_xLa_{1-x} changes from clustering of the same kind of atoms ($\eta^0 < 0$) to the chemical preference of the different atoms ($\eta^0 > 0$) with increasing Fe concentration. Table 2 also includes values of the full width of the half maximum (FWHM) of the three nearest-neighbour correlation peaks in the $G(r)$ curve. The present values in table 2 are a little different from the previous ones (Matsuura *et al* 1988b) because of an improvement of data analysis; an elimination of inelastic scattering contribution due to utilising a monochromator is taken into account in the present work.

3.2. Small-angle x-ray scattering

Plots of $\log P_c(Q)$ against $\log Q$ for a-Fe_xLa_{1-x} ($x = 0.7$, 0.8 and 0.9) alloys are shown in figure 6. The small-angle scattering intensity for the alloy with $x = 0.9$ is larger than for those with $x = 0.8$ and 0.7 by more than two orders of magnitude. Figure 6 indicates that there are two regions where the $P_c(Q)$ is represented as a different power of Q for a-$Fe_{0.9}La_{0.1}$. Plots of the logarithm of the absolute intensity, $\log J(Q)$, against Q^2 (i.e.

Table 2. Structural parameters determined from x-ray diffraction of a-Fe_xLa_{1-x} alloys. The order parameter η and normalised order parameter η^0 are defined by Cargill and Spaepen (1981).

	Interatomic distance (Å)												
	1st-nearest neighbour			2nd-nearest neighbour			Coordination number			Order parameter		FWHM-of 1st nearest neighbour peak in $G(r)$ (Å)		
x in Fe_xLa_{1-x}	Fe–Fe	Fe–La	La–La	4th	5th	6th	Fe–Fe	Fe–La	La–La	η	η^0	Fe–Fe	Fe–La	La–La
0.90	2.542	3.161	3.774	4.143	4.516	4.982	8.55	2.24	3.47	0.061	0.250	0.37	0.62	0.31
0.85	2.536	3.161	3.731	4.189	4.584	5.001	7.78	2.72	4.10	0.049	0.149	0.35	0.60	0.42
0.75	2.566	3.193	3.702	4.059	4.387	4.954	6.92	3.51	5.19	0.064	0.013	0.34	0.63	0.55
0.67	2.571	3.240	3.696	4.243	*	4.908	6.27	3.51	5.62	−0.085	−0.132	0.37	0.52	0.43
0.65	2.545	3.168	3.624	3.923	4.246	4.869	6.28	3.00	6.20	−0.204	−0.299	0.36	0.53	0.47

* Cannot be distinguished.

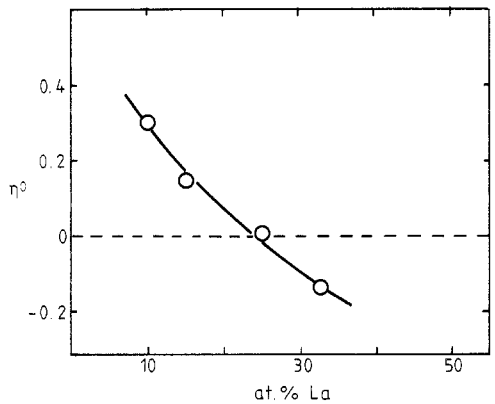

Figure 5. The normalised order parameter η^0 plotted against La concentration for amorphous Fe_xLa_{1-x} alloys.

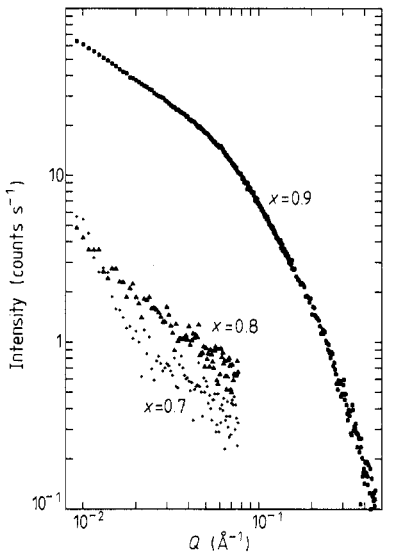

Figure 6. Log–log plot of x-ray small-angle scattering intensity $P_c(Q)$ against Q for amorphous Fe_xLa_{1-x}(x = 0.7, 0.8 and 0.9) alloys.

Guinier plots) are shown in figure 7 for a-$Fe_{0.9}La_{0.1}$. The results indicate that a unique radius of gyration for a-$Fe_{0.9}La_{0.1}$ alloy cannot be determined, which may suggest a wide distribution of the particle size. The correlation function $\gamma(r)$ for a-$Fe_{0.9}La_{0.1}$ was deduced from the absolute scattering intensity $J(Q)$ using equation (6) and is shown in figure 8. Though a definite correlation length cannot be defined from the $\gamma(r)$ curve just as a unique radius of gyration cannot from the Guinier plot, the correlation length ranges from 40 to 120 Å. The $\gamma(0)$-value estimated from the absolute intensity $J(Q)$ using equation (7) leads to 0.24×10^{46} (eu^2 cm^{-6}) for a-$Fe_{0.9}La_{0.1}$.

4. Discussion

As described earlier, the ferromagnetic state of a-Fe_xLa_{1-x} alloys becomes unstable with increasing Fe concentration, and finally at 90 at.% Fe the AC susceptibility in a weak field shows a cusp typical of a spin glass. The interatomic distances between Fe–Fe and Fe–La atoms are shortened slightly with increasing Fe concentration, while that of La–La atoms is elongated, as shown in figure 3. The Fe–Fe interatomic distance of γ-Fe precipitated in Cu is 2.529 Å at 70 K (Gonser *et al* 1963) and the critical Fe–Fe interatomic distance at which an antiferromagnetic coupling competes with a ferromagnetic one has been estimated as 2.54 Å (Forrester *et al* 1979). The alloys of a-Fe_xLa_{1-x} ($0.65 \leqslant x \leqslant 0.9$) have Fe–Fe interatomic distances close to the critical value, as shown in table 2. Therefore, ferromagnetic states of a-$Fe_{0.9}La_{0.1}$ are inclined to be unstable. Another important effect of the Fe–Fe interatomic distance on the ferromagnetic instability is a distance fluctuation around the mean value i.e. $\sqrt{(\delta r_1)^2}/r_1$, where r_1 is the position of Fe–Fe first-neighbour peak in $G(r)$. The greater the fluctuation is, the more unstable a ferromagnetic state becomes. The estimated value of $\sqrt{(\delta r_1)^2}/r_1$ for $Fe_{0.9}La_{0.1}$ from the Fe–Fe peak in $G(r)$ is 0.478 Å. This value is close to the critical value above which

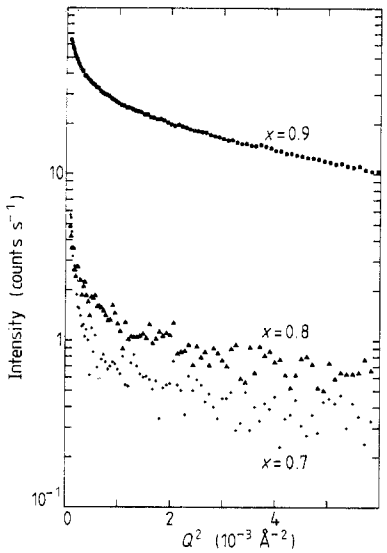

Figure 7. The absolute intensity of small-angle x-ray scattering ($\log J(Q)$) plotted against Q^2 (Guinier plot) for amorphous $Fe_{0.9}La_{0.1}$ alloy.

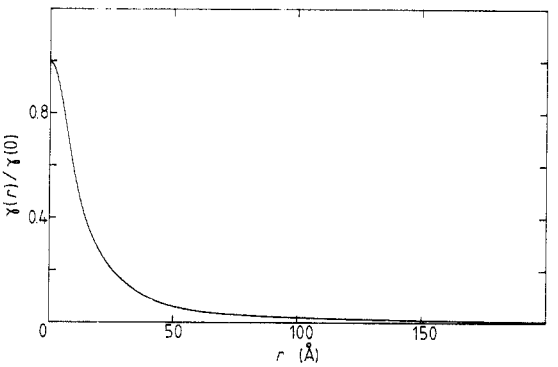

Figure 8. The correlation function $\gamma(r)$ for amorphous $Fe_{0.9}La_{0.1}$ alloy.

ferromagnetic states of pure iron turn out to be unstable and spin glass states appear (Kakehashi 1988).

The magnetic state of Fe-rich a-Fe_xLa_{1-x} must be affected not only by the Fe–Fe interatomic distance but also by the Fe–Fe coordination. The three partial coordination numbers of Fe–Fe, Fe–La and La–La pairs vary monotonically with Fe concentration. The present results indicate that the magnetic properties of a-Fe_xLa_{1-x} are strongly correlated with the Fe–Fe coordination as will be described below.

It is instructive to compare the magnetic properties of a-$Fe_{0.9}La_{0.1}$ alloy with those of crystalline $(Fe_xAl_{1-x})_{13}La$ alloys. Crystalline $(Fe_xAl_{1-x})_{13}La$ alloys exhibit three different magnetic states depending on the iron concentration: (i) a micto magnetic state ($0.46 \leqslant x < 0.62$), (ii) a soft ferromagnetic state ($0.62 < x \leqslant 0.86$) and (iii) an antiferromagnetic state ($0.86 < x \leqslant 0.92$) (Palstra *et al* 1985). There are two different iron sites in the $(Fe_xAl_{1-x})_{13}La$ alloys i.e. Fe^{I} and Fe^{II}. Both sites have high coordination number, 12 and 10 for Fe^{I} and Fe^{II}, respectively. With increasing iron concentration, the mean Fe–Fe coordination number increases up to 10.2 for $x = 1$. Under such a high coordination, the ferromagnetic ordering collapses and an antiferromagnetic state appears. It is very interesting to note that the ferromagnetic state of c-$(Fe_xAl_{1-x})_{13}La$ alloys transforms into the antiferromagnetic one at an Fe–Fe coordination of 8.8 which is close to the present value of 8.6 where the a-Fe_xLa_{1-x} alloy exhibits a cusp typical of a spin glass in AC susceptibility. Therefore, the Fe–Fe coordination number 8.6–8.8 may be the critical value below which ferromagnetic long-range order is stable and above which an antiferromagnetic coupling should prevail. Though ferromagnetic states for both alloys turn out to be unstable with increasing iron concentration toward pure iron, neither an antiferromagnetic long-range order nor a sharp spin flip occurs in a-$Fe_{0.9}La_{0.1}$ unlike in c-$(Fe_xAl_{1-x})_{13}La$. These differences can be ascribed mainly to the disordered structure of a-Fe_xLa_{1-x} alloys because a long-range antiferromagnetic structure cannot

be established in the disordered structure such as amorphous alloys exhibiting a spin frustration (Kaneyoshi 1983). Furthermore, the Fe–Fe interatomic distance for a-$Fe_{0.9}La_{0.1}$ (=2.542 Å) is not so short as that for c-$(Fe_xAl_{1-x})_{13}La$ (=2.445 Å for x = 0.86). Therefore an antiferromagnetic coupling for a-$Fe_{0.9}La_{0.1}$ should be weaker than for c-$(Fe_xAl_{1-x})_{13}La$.

We can reasonably expect that the considerably high intensity of the small-angle scattering correlates with the spin-glass-like behaviour for a-$Fe_{0.9}La_{0.1}$. Since SAXS reflects a structure of medium-range order, the fairly large SAXS intensity found in a-$Fe_{0.9}La_{0.1}$ alloy means that there are particles with different electron densities from surrounding matrix. The size of the particles can be estimated to be 40–120 Å from the $\gamma(r)$ curve. There are three possible causes of such an electron density fluctuation: the existence of (i) an Fe-rich region, (ii) a La-rich region and (iii) their mixture. The third case is out of numerical treatment. As an extreme case, if a-$Fe_{0.9}La_{0.1}$ were to be phase-separated into two pure elements, the $\gamma(0)$-value could be easily estimated assuming each phase had the same electron density as the crystalline one, i.e. BCC Fe or HCP La. The calculated $\gamma(0)$-value (25×10^{46} eu^2 cm^{-6}) is about 100 times greater than the experimental one. Furthermore, the results of the order parameters η^0 shown in figure 5 suggest that the structure of a-$Fe_{0.9}La_{0.1}$ exhibits chemical preference for Fe–La neighbours rather than clustering. Therefore, it is implausible that La atoms in a-$Fe_{0.9}La_{0.1}$ would be concentrated into clusters. Alternatively, most of the matrix is assumed to be homogeneous and only a small number of Fe atoms cluster, whose short-range structure must be similar to that of FCC γ-Fe. In this case the average electron density ρ_a and density fluctuation $\Delta\rho$ can be denoted as

$$\rho_a = V_f\rho_{\gamma\text{-Fe}} + (1 - V_f)\rho_0 \tag{11}$$

and

$$\Delta\rho = \rho_{\gamma\text{-Fe}} - \rho_0 \tag{12}$$

where $\rho_{\gamma\text{-Fe}}$ and V_f are the electron density of the γ-Fe-like particles and their volume fraction, respectively, and ρ_0 the electron density in the homogeneous part. The volume fraction V_f can be evaluated from equations (8), (11) and (12), and the $\gamma_{exp}(0)$ i.e.

$$V_f = \gamma_{exp}(0)/[(\rho_a - \rho_{\gamma\text{-Fe}})^2 + \gamma_{exp}(0)]. \tag{13}$$

The electron density of γ-Fe, $\rho_{\gamma\text{-Fe}}$, is estimated by extrapolating the lattice constant (Pearson 1958) down to the room temperature (20 °C) and ρ_a, from the density measurement, i.e. $\rho_{\gamma\text{-Fe}} = 2.31 \times 10^{48}$ (eu cm^{-3}) and $\rho_a = 1.95 \times 10^{48}$ (eu cm^{-3}). The resultant V_f-value is 0.019, namely about 2% of the total volume. Therefore, we can conjecture that the a-$Fe_{0.9}La_{0.1}$ alloy contains Fe-concentrated regions 40–120 Å in size and about 2% of total volume, where an antiferromagnetic coupling dominates because of the high Fe–Fe coordination and the spin frustration due to a topological constriction (Kaneyoshi 1983).

Since the composition of a-$Fe_{0.9}La_{0.1}$ is close to the critical concentration region where an amorphous state can be formed by sputtering, a structural or a compositional fluctuation is likely to occur. Therefore, iron clusters are apt to be formed in a concentration region near pure iron. These iron clusters in a-$Fe_{0.9}La_{0.1}$ must affect the magnetic state of the surrounding matrix through their boundaries. The ferromagnetic state of the matrix itself is unstable because the Fe–Fe coordination is relatively large and the Fe–Fe interatomic distance is close to the critical value of 2.54 Å. Therefore, the iron clusters where antiferromagnetic couplings prevail against ferromagnetic ones

work to enhance the ferromagnetic instability and lead to the appearance of the spin glass state of a-$Fe_{0.9}La_{0.1}$.

5. Summary

The results of large-angle x-ray scattering for a-Fe_xLa_{1-x} alloys indicate the following: (i) the Fe–Fe interatomic distances are close to the critical value of a competition between ferro- and antiferromagnetic exchanges, (ii) the Fe–Fe coordination number increases with Fe concentration and reaches 8.55 for $x = 0.9$, and (iii) the fluctuation of the Fe–Fe interatomic distance is largest for the alloy with $x = 0.9$. These facts suggest that an antiferromagnetic coupling prevails against a ferromagnetic one with increasing Fe concentration and finally a spin glass state appears at $x = 0.9$.

The results of small-angle x-ray scattering for a-Fe_xLa_{1-x} show that there are inhomogeneous regions probably consisting of iron clusters in a-$Fe_{0.9}La_{0.1}$ but not in other alloys. This implies that iron clusters in a-$Fe_{0.9}La_{0.1}$ are associated with the spin glass behaviour of this alloy; iron clusters can enhance the instability of ferromagnetic couplings in the matrix.

Acknowledgments

Two of the authors, MM and KF, owe this work to the financial support by Grant-in-Aid for Scientific Research Project Nos 63850155 and 63460190, respectively, from the Ministry of Education, Japan.

References

Cargill III G S and Spaepen F 1981 *J. Non-Cryst. Solids* **43** 91–5
Forrester D W, Koon N C, Schelleng J H and Rhyne J J 1979 *J. Appl. Phys.* **50** 7336–41
Fukamichi K 1983 *Amorphous Metallic Glasses* ed. F E Luborsky (London: Butterworths) pp 318–40
Fukamichi K and Hiroyoshi H 1985 *Sci. Rep. RITU* A **32** 154–67
Fukamichi K, Komatsu H, Goto T and Wakabayashi H 1988 *Physica* B **149** 276–80
Fukamichi K, Komatsu H, Goto T, Wakabayashi H and Matsuura M 1989 *MRS Int. Meeting, Tokyo* at press
Gonser U, Meechan C J, Muir A H and Wiedersich H 1963 *J. Appl. Phys.* **24** 2373–8
Guinier A and Fournet G 1955 *Small Angle Scattering of X-rays* (New York: Wiley) pp 111–20
Kakehashi Y 1988 private communication
Kaneyoshi T 1983 *Glassy Metals* ed. R Hasegawa (Boca Raton, FA: CRC) pp 37–64
Matsuura M, Fukunaga R, Fukamichi K, Sato Y and Suzuki K 1988a *Z. Phys. Chem. NF* **157** 85–9
Matsuura M, Fukunaga T, Fukamichi K and Suzuki K 1988b *Solid State Commun.* **66** 333–7
Palstra T T M, Nieuwenhuys G J, Mydosh J A and Buschow K H J 1985 *Phys. Rev.* B **31** 4622–32
Pearson W B 1958 *A Handbook of Lattice Spacings and Structures of Metals and Alloys* (Oxford: Pergamon) p 625
Saito N, Hiroyoshi H, Fukamichi K and Nakagawa Y 1986 *J. Phys. F: Met. Phys.* **16** 911–9
Schmidt P W 1976 *Crystallographic Computing Techniques* ed. F R Ahmed, K Huml and B Sedlacek (Copenhagen: Munksgaard) pp 363–75
Wakabayashi H 1988 *Doctoral Thesis* Tokyo Institute of Technology